# Calorimetric study of the crystallization kinetics of $Cu_{47}Ti_{33}Zr_{11}Ni_8Si_1$ metallic glass

S. Venkataraman,[1,2,*] H. Hermann,[2] C. Mickel,[2] L. Schultz,[2] D. J. Sordelet,[3] and J. Eckert[2]
[1]*FG Physikalische Metallkunde, FB 11 Material- und Geowissenschaften, Technische Universität Darmstadt, Petersenstraße 23, D-64287 Darmstadt, Germany*
[2]*Leibniz-Institut für Festkörper- und Werkstoffforschung Dresden, Helmholtzstraße 20, D-01069 Dresden, Germany*
[3]*Material and Engineering Physics Program, Ames Laboratory (USDOE), Iowa State University, Ames, Iowa 50014, USA*
(Received 14 October 2006; revised manuscript received 1 December 2006; published 27 March 2007)

The isochronal and isothermal activation energies for the primary crystallization process of $Cu_{47}Ti_{33}Zr_{11}Ni_8Si_1$ metallic glass powders subjected to varying thermal treatments have been evaluated by differential scanning calorimetry and determined using the Kissinger approach and the Johnson-Mehl-Avrami (JMA) analysis, respectively. The values of the differential Avrami exponent are also determined from the isothermal data. Assuming diffusion-controlled growth, it is shown that thermal treatment of the samples in the supercooled liquid region considerably influences the behavior of the nucleation rate during the crystallization process. Microstructural investigations indicate that the thermal treatment is accompanied by precipitation of fine nanocrystals in an amorphous matrix. The values for the activation energies determined by both the Kissinger approach and the JMA analysis are similar for the as-prepared powder, but a significant difference is found for the thermally treated powders. This discrepancy is explained on the basis of the fundamental assumptions made in the models. It will be shown that the Kissinger method fails if the differential Avrami exponent changes significantly during the transformation process.

DOI: 10.1103/PhysRevB.75.104206 PACS number(s): 81.05.Kf, 68.55.Ac, 68.60.Dv, 64.70.Dv

## I. INTRODUCTION

It has long been recognized that many technologically important properties of materials, such as their mechanical strength and toughness, creep and corrosion resistance, or magnetic and superconducting properties, are essentially controlled by the presence of precipitated particles of a second phase.[1,2] An important part of the recent developments corresponds to nanostructured materials obtained by controlled crystallization, either by annealing an amorphous single phase or by decreasing the cooling rate upon quenching the liquid of metallic systems.[3] The kinetic behavior associated with a structural change leading to an alternative metastable state in a glassy alloy above its glass transition is a key subject since it provides new opportunities for structure control by innovative design and processing strategies.[4,5] Several examples for such structure control include hard[6] and soft[7] magnets as well as high-strength materials.[8]

Controlling the microstructure development from amorphous precursors requires detailed understanding of the specific mechanisms influencing structural transformations.[1,9] Thermal analysis tools, in particular differential scanning calorimetry (DSC), have been successfully employed for studying the phase transformations involving nucleation and growth[10] and continuous grain growth of preexisting nuclei[10] and for investigating the crystallization kinetics of glass-forming liquids.[11–18] Kinetic data on first-order transformations are often obtained from this technique in either isothermal or linear heating (isochronal) mode.[19] While isothermal analyses are in most cases more definitive, it has been shown that the nonisothermal technique also has several advantages,[20] in particular that experiments can be performed quite rapidly. Additionally, many phase transformations occur too rapidly to be measured under isothermal conditions because of transients associated with the experimental apparatus.[20]

For the isochronal process, the Kissinger relation,[21] described later in the Results section, is frequently used to determine the activation energy of a specific transformation. Although the Kissinger analysis was not originally developed for solid-state transformations, Henderson[20] has shown that it is applicable. The activation energy calculated using the Kissinger approach depends on the temperature dependences of the nucleation and growth rates and on any transient events, which they may exhibit. Despite difficulty in interpretation, this approach has been widely used for comparing the stability of metallic glasses. Conversely, one of the legacies of the classic work done by Kolmogorov,[22] Johnson and Mehl,[23] and Avrami[24] concerning the kinetics of phase transformations involving nucleation and growth under isothermal conditions is the Johnson-Mehl-Avrami (JMA) transformation equation. Using the JMA equation, described later in the Results section, the reaction rate as well as parameters governing the nucleation rate and/or the growth morphology can be obtained.[25] Calka and Radlinski,[26] however, have shown that the usual method of calculating a mean value of the Avrami exponent over a range of transformed volume fraction may be inappropriate or even misleading in the case where competing reactions or changes in growth dimensions occur during the progress of the transformation. They derived a more sensitive approach by plotting the first derivative of the Avrami plot against the transformed volume fraction which gives the differential (or local) value of the Avrami exponent.[27,28] Such a differential Avrami plot can highlight changes in reaction kinetics during the progress of transformation.[29]

$Cu_{47}Ti_{33}Zr_{11}Ni_8Si_1$ is one of the best glass-forming alloys in the Cu-Ti-Ni-Zr system and has a high resistance against crystallization and displays a wide supercooled liquid region prior to the onset of crystallization.[30] The crystallization kinetics of $Cu_{47}Ti_{33}Zr_{11}Ni_8Si_1$ metallic glass powders prepared by gas atomization was studied earlier, and it was shown that

 

crystallization occurs with an increasing nucleation rate and the transformation is governed by diffusion controlled three-dimensional growth.[31] However, not much is known about the crystallization behavior of this alloy upon thermal treatment at temperatures in the supercooled liquid region. An earlier atom probe tomography (APT) study on the crystallization of $Cu_{47}Ti_{33}Zr_{11}Ni_8Si_1$ metallic glass has shown that this glassy composition undergoes amorphous phase separation into copper-enriched and titanium-enriched regions prior to the formation of nanocrystals.[32] The influence of such a preceding amorphous phase separation on understanding the kinetics and thermodynamics of the crystallization mechanism has been studied in various Zr-Ti-Cu-Ni-Be glass-forming compositions and also in $Pd_{43}Ni_{10}Cu_{27}P_{20}$ metallic glass.[13,15–17] A previous study by the authors has found no evidence for amorphous phase separation occurring prior to crystallization in the $Cu_{47}Ti_{33}Zr_{11}Ni_8Si_1$metallic glass.[33] However, only a transmission electron microscope (TEM) was employed.[33] It is well known that APT can be used to verify possible compositional fluctuations on an atomic scale in a given volume with great precision, a feature which cannot be studied using a conventional TEM.[34] Additionally, it is well known that crystallization can proceed through multiple pathways which depend on annealing temperature.[35,36]

The present paper will discuss the results on the crystallization kinetics of the $Cu_{47}Ti_{33}Zr_{11}Ni_8Si_1$ metallic glass powders. Thermal treatment of the as-prepared powders in the supercooled liquid region can possibly influence the crystallization mechanism and is investigated. Experimental measurements include DSC operated under isochronal and isothermal modes. Additionally, systematic microstructural observations on the thermally treated $Cu_{47}Ti_{33}Zr_{11}Ni_8Si_1$ metallic glass powders have been carried out using a TEM as well as x-ray diffraction (XRD). The kinetics of crystallization is analyzed within the framework of the Kissinger approach, the JMA analysis as well as the differential Avrami analysis. The considerable scatter observed in the values of the activation energies calculated for the thermally treated powders is explained on the basis of the central assumptions made in the models. Using model calculations we attempt to clarify the observed behavior.

## II. EXPERIMENTAL PROCEDURE

Powders of nominal composition $Cu_{47}Ti_{33}Zr_{11}Ni_8Si_1$ were produced by high-pressure Ar gas atomization. The details of powder synthesis are reported elsewhere.[33] The nominal size of the powders used in the present study was 20 $\mu$m. Structural characterization was performed by XRD using a Philips PW1050 diffractometer (Co $K\alpha$ radiation). Microstructural characterization as well as energy-dispersive x-ray analysis (EDX) was carried out on ion-milled powder samples using a JEOL 2000 FX TEM operated at 200 kV accelerating voltage. Ion milling (3 kV, 3 mA, and 7°) was performed using a stage cooled by liquid nitrogen. This was achieved using a BAL-TEC RES 101 rapid etching system. Powder particles were embedded in a mixture of epoxy resin and TiN filler powder and subsequently cured, resulting in a compact material. Slices were then cut from this compact and finally polished down to a thickness of few microns prior to ion milling. Thermal treatment of the powder samples as well as calorimetric studies was done using a Perkin Elmer DSC 7 DSC under high-purity flowing Ar. Aluminum pans were used as sample holders. The isochronal DSC measurements were made at heating rates ranging from 10 K/min to 80 K/min. For the isothermal DSC measurements, the samples were first heated to a fixed temperature at a heating rate of 40 K/min and held for a certain period of time. For all the DSC runs, two successive runs were recorded with the second run serving as a baseline. The calorimeter was calibrated for temperature and energy at various heating rates with high purity indium and zinc standards, giving an experimental error for the temperature and the enthalpy of about 1 K and 0.5 J/g, respectively.

This study deals with four different $Cu_{47}Ti_{33}Zr_{11}Ni_8Si_1$ powder samples. A brief description of each individual sample as well as its thermal history is necessary and is given here.

*Sample A*: the gas atomized $Cu_{47}Ti_{33}Zr_{11}Ni_8Si_1$ powder in the as-prepared state.

*Sample B*: $Cu_{47}Ti_{33}Zr_{11}Ni_8Si_1$ powder thermally treated up to 708 K. The thermal treatment involved constant-rate heating the powder up to 708 K at a heating rate of 40 K/min followed by cooling down to room temperature at 100 K/min.

*Sample C*: $Cu_{47}Ti_{33}Zr_{11}Ni_8Si_1$ powder treated up to 733 K. For this type of sample, a similar DSC scheme as for sample *B* has been done, except that the powder was heated up to 733 K.

*Sample D*: $Cu_{47}Ti_{33}Zr_{11}Ni_8Si_1$ powder thermally treated up to 743 K; i.e., a similar DSC procedure has been done as for samples *B* and *C* but a final temperature of 743 K was used in this case.

## III. RESULTS

### A. Constant heating rate analysis

Figure 1(a) shows the constant-heating-rate (40 K/min) DSC plots of the different samples. All specimens exhibit a distinct endotherm, characteristic of a glass transition prior to the crystallization exotherm. The thermal stability data are represented by $T_g$, $T_x$, and $\Delta T$, where $T_g$ is the glass transition temperature (defined as the onset of the endothermic event), $T_x$ is the crystallization onset temperature, and $\Delta T$ is the extent of supercooled liquid region ($\Delta T = T_x - T_g$). The values of $T_g$, $T_x$, and $\Delta T$ for all the samples at a heating rate of 40 K/min are determined to be 700, 762, and 62 K, respectively. These values are in good agreement with those reported earlier for a bulk metallic glass of the same composition.[30] A look at the DSC traces for the thermally treated samples reveals no significant difference in comparison with the as-prepared powder. Figure 1(b) shows the DSC traces of the different samples in the temperature range 350–755 K. It is clearly visible that the as-prepared powder (sample *A*) shows a broad exothermic event in the temperature range 450–700 K. Isochronal thermal treatment (done for samples *B*, *C*, and *D*) leads to the disappearance of this exothermic event.

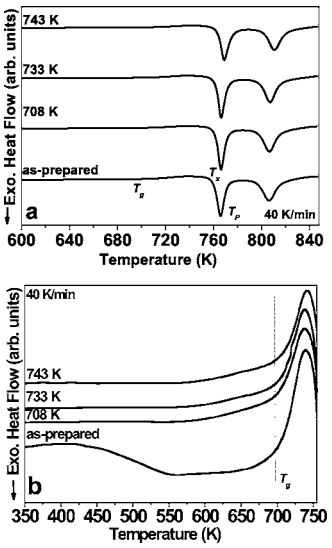


FIG. 1. DSC traces (heating rate 40 K/min) for as-prepared and thermally treated $Cu_{47}Ti_{33}Zr_{11}Ni_8Si_1$ powders within the range of (a) 600–840 K and (b) 350–755 K.

To obtain the activation energy from the Kissinger plot, isochronal DSC runs at different heating rates (10, 20, 30, 40, 60, 80 K/min) were performed on all powder samples. Subsequently, the characteristic peak temperatures were derived from these DSC measurements. The Kissinger plots were derived from the Kissinger equation,[21] which is expressed as

$$\ln(\Phi/T_P^2) = -(E_{Kissinger}/RT_P) + c, \tag{1}$$

where $\Phi$ is the heating rate and $T_P$ is the characteristic peak temperature corresponding to the first exothermic event, as seen in Fig. 1(a), $E_{Kissinger}$ is the activation energy, $R$ is the gas constant, and $c$ is a constant. By plotting $\ln(\Phi/T_P^2)$ against $(1/T_P)$ one can derive the value of $E_{Kissinger}$ from the slope of the straight line plotted. Figure 2 shows the Kissinger plot for the powders. The Kissinger activation energies of the powder samples are listed in Table I. Increasing the thermal treatment temperature does not seem to have a significant effect on the value of the Kissinger activation energy since the values obtained are within the error limits.

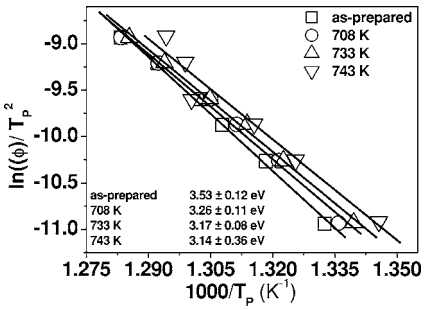


FIG. 2. Kissinger plots for the as-prepared and thermally treated $Cu_{47}Ti_{33}Zr_{11}Ni_8Si_1$ powders.

TABLE I. Activation energies and Avrami exponent for $Cu_{47}Ti_{33}Zr_{11}Ni_8Si_1$ powders.

| Sample condition | $E_{Kissinger}$ (eV) | $E_{isothermal}$ (eV) | Avrami exponent ($n$) at 733 K ($0.10 \leq X \leq 0.85$) |
|---|---|---|---|
| As-prepared | 3.53±0.12 | 3.69±0.21 | 3.42±0.06 |
| 708 K | 3.26±0.11 | 4.28±0.14 | 3.20±0.05 |
| 733 K | 3.17±0.08 | 4.56±0.21 | 3.03±0.06 |
| 743 K | 3.14±0.36 | 4.59±0.22 | 2.65±0.06 |

### B. Isothermal analysis

Figure 3 shows the isothermal DSC traces at 733 K for all the different powder samples. It is evident that all curves display an exotherm after certain incubation time. Additionally, it is clear that the incubation time decreases with increasing thermal treatment temperature. It is assumed that the volume fraction of transformed material $X$, up to any time $t$, is proportional to the fractional area of the exothermic peak. Hence, the crystallized volume fraction can be accurately determined by measuring the partial area of the exothermic signal. The results obtained for samples $A$–$D$ are shown in Fig. 4, displaying a typical sigmoidal-type curve for the crystallized volume fraction as a function of annealing time. It can be observed that the curves become a little bit steeper with increasing pretreatment temperature and indicate that the thermally treated specimens transform at a faster rate compared to the as-prepared powder.

In the theory of the solid-state phase transformation, the JMA equation is widely used in modeling the isothermal phase transformation mechanism.[25] The JMA equation relates the transformed volume fraction $X$ at a constant annealing temperature $T$ and time $t$:

$$X(t) = 1 - \exp\{-[K_T(t - t_0)]^n\}, \tag{2}$$

where $K_T$ is a temperature-dependent kinetic constant, $t_0$ is the incubation time for the process, and $n$ is an exponent, which represents the transformation behavior (the "Avrami exponent"). This kinetic parameter has proved to be significant in describing the transformation mechanism, such as the nucleation and growth behavior.[37] Figure 5 shows the JMA plot for the powder samples measured at 733 K. For the transformation range under consideration ($0.10 \leq X \leq 0.85$), the plot shows almost a straight-line behavior. The Avrami

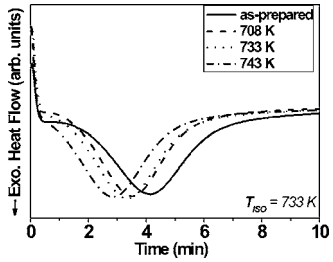


FIG. 3. Isothermal DSC traces at 733 K for as-prepared and thermally treated $Cu_{47}Ti_{33}Zr_{11}Ni_8Si_1$ powders.

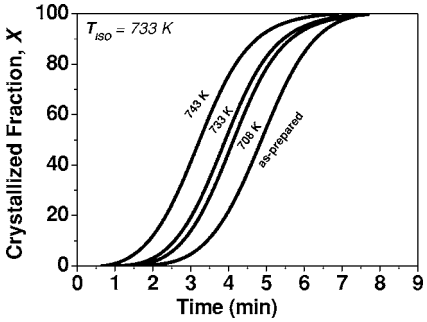


FIG. 4. Crystallized volume fraction versus time at 733 K for as-prepared and thermally treated $Cu_{47}Ti_{33}Zr_{11}Ni_8Si_1$ powders.

exponent $n$ is calculated from Fig. 5 by approximating the data by a straight line. It can be seen that the Avrami exponent decreases from 3.4 for the as-prepared powder to about 2.6 for the powder treated up to 743 K.

Normally, for the isothermal crystallization process of an amorphous alloy, a mean value of the Avrami exponent has been used to interpret the process.[25] However, Calka and Radlinski[26] have proposed an alternative analysis method of the isothermal DSC results for the crystallization of amorphous alloys. It is based on examining the differential value of the Avrami exponent versus the crystallized volume fraction $X$. The differential Avrami exponent $n(X)$ is defined as

$$n(X) = \partial \ln[-\ln(1-X)]/\partial \ln(t-t_0). \tag{3}$$

Figure 6 shows the plot of $n(X)$ vs $X$ in a range 0–100%. It is clear that the value of $n(X)$ does not remain constant over the whole transformation range. For the as-prepared powder, it increases from about 2.5 at the beginning of crystallization to a maximum value of 3.4 and remains more or less constant for most part of the transformation. However, for the powder treated at 708 K it is found that although there is an initial increase from about 2.5 to 3.2 until 40% of the crystallization has occurred, there is a steep decrease in the value of the differential Avrami exponent to about 2.3 at around 95% crystallization. Similar observations can also be made for the powder samples treated at 733 K and 743 K where a decrease of the $n(X)$ value occurs as the crystallization proceeds. Also visible from Fig. 6 is the fact that the differential Avrami exponent increases to higher values in the final stages of crystallization ($X > 95\%$).

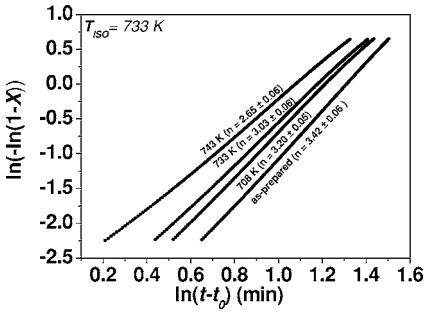


FIG. 5. Avrami plots ($0.10 \leq X \leq 0.85$) at 733 K for $Cu_{47}Ti_{33}Zr_{11}Ni_8Si_1$ alloy powders.

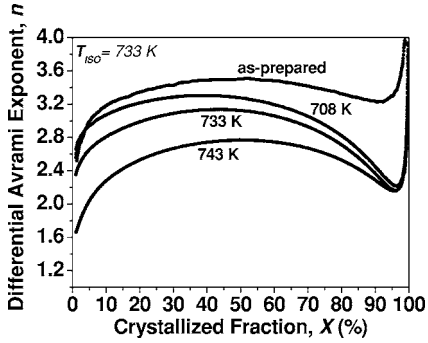


FIG. 6. Variation of the differential Avrami exponent with crystallized volume fraction for as-prepared and thermally treated $Cu_{47}Ti_{33}Zr_{11}Ni_8Si_1$ powders at 733 K. The deviation of the calculation is within 5% when $X$ is 5–95% but more when $X$ is either $\leq 5\%$ or $\geq 95\%$.

The reaction rate constant $K_T$ is a function of annealing temperature and can be calculated from the intercept of the JMA plots (Fig. 5). Under isothermal conditions, the Arrhenius equation is often used to calculate the activation energy for crystallization of an amorphous alloy:[19]

$$K_T = K_0[\exp(-E_{isothermal}/RT)], \tag{4}$$

where $K_0$ is a constant and $E_{isothermal}$ is the apparent activation energy for crystallization. Figure 7 shows the plot of $\ln(K_T)$ vs $(1/T)$, which also yields a straight line. The activation energies calculated thereby are listed in Table I. The isothermal activation energy shows and increasing trend with a value of 3.69 eV for the as-prepared powder as compared with the value of 4.59 eV for the powder treated at 743 K.

### C. Structural and microstructural analysis

Figure 8 shows the XRD patterns of the powder samples $A$–$D$. The XRD patterns are typical of an amorphous material. No indication of crystallinity was found within the detection limits of XRD. Figure 9 shows the TEM images for samples $A$, $B$, and $D$. The bright field (BF) image and the dark field (DF) image of sample $A$ are typical of an amorphous material. Additionally, the selected area diffraction (SAD) pattern (shown as an inset) shows diffuse rings, characteristic of an amorphous structure. In the case of sample $B$ the BF as well as DF images clearly show the presence of

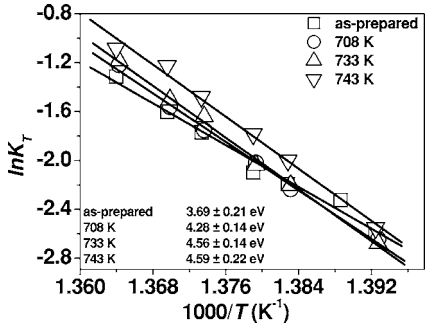


FIG. 7. Arrhenius plot for the isothermal activation energy of as-prepared and thermally treated $Cu_{47}Ti_{33}Zr_{11}Ni_8Si_1$ powders.

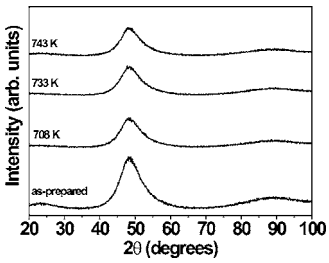


FIG. 8. XRD patterns of as-prepared and thermally treated $Cu_{47}Ti_{33}Zr_{11}Ni_8Si_1$ powders.

nanocrystals of about 5 nm. This is also corroborated with the diffraction pattern where the rings are well defined. A faint halo still exists which overlaps with the rings. This indicates that the thermal treatment at 708 K (sample *B*) results in the formation of crystalline nuclei though a substantial amount of the amorphous phase still exists. In the case of sample *D* the SAD pattern of sample clearly reveals the formation of solid lines and sharp spots indicating increased volume fraction of the nanocrystalline phase. The size of the bright spots in the DF image is in the range of 5–10 nm and correlates well with the regions of nonuniform intensity as seen in the corresponding BF image. Visual inspection of the TEM patterns suggests that bulk average size and number of crystallites increases with the temperature of thermal treatment. Quantitative estimates for the volume fraction of the crystallites can, however, not be made. From the comparison of the shape of the XRD curves we conclude that this volume fraction does not exceed the order of 1%. EDX analysis indicates that these nanocrystals tend to be richer in Cu than the surrounding matrix. However, clear indexing of the nanocrystals was not possible because of their small size.

## IV. DISCUSSION

The XRD profiles (Fig. 8) as well as the isochronal DSC scans (Fig. 1) clearly display the features that are typical of a metallic glass. All the DSC traces show a distinct endotherm, characteristic of a supercooled liquid prior to the appearance of the exothermic crystallization events which represent the devitrification of the metallic glass. The amorphous nature of the as-prepared powder has been also verified using TEM.

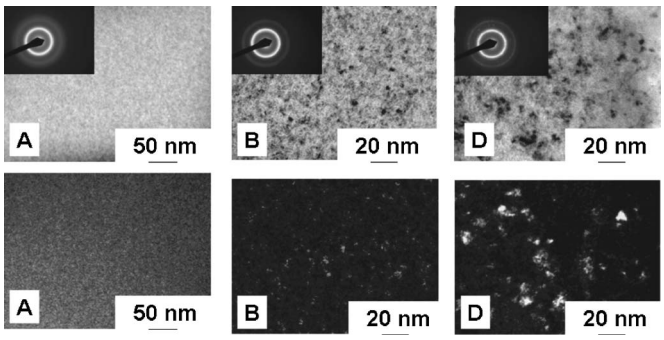


FIG. 9. Bright field TEM image with diffraction pattern as inset and dark field image of $Cu_{47}Ti_{33}Zr_{11}Ni_8Si_1$ powders. The caption denotes sample identification (refer to the Experiment section).

The as-prepared powder exhibits a broad exothermic event preceding the main endothermic and exothermic events. The origin of this exotherm has been found to stem from structural relaxation as well as nanocrystallization.[33] TEM studies (Fig. 9) show that the thermal treatment at 708 K and 743 K results in the formation of nanocrystals in an amorphous matrix. Hence, the thermal treatment at temperatures in the supercooled liquid region, as has been done in the present study, results in the formation of nuclei. However, the XRD patterns for the thermally treated powders do not reveal any crystallinity. This could be because it is well known that XRD patterns for grains less than 5 nm also reveal a broad halo.[38]

A previous study of the crystallization of $Cu_{47}Ti_{33}Zr_{11}Ni_8Si_1$ metallic glass has shown that the crystallization is primary in nature and the product of the primary crystallization is the hexagonal $Cu_{51}Zr_{14}$ phase.[33] Primary crystallization can be defined as the formation of a product (crystalline phase) with a composition different from the parent (glassy) phase.[39] Accordingly, the formation of the primary crystallization product changes the composition of the remaining amorphous phase. This includes the fact that the crystallization process starts at nucleation centers where the local chemical composition should be similar to that of the crystallites generated—i.e., $Cu_{51}Zr_{14}$ in the present case. Since the enthalpy of mixing of Cu-Zr pairs is −23 kJ/mol and that of Cu-Ti as well as that of Ti-Zr are −9 kJ/mol and 0 kJ/mol, respectively,[40] it is clear that the Cu-rich regions that develop prior to the formation of the $Cu_{51}Zr_{14}$ phase are also zirconium enriched.

The present isothermal analysis of the powders gives a more detailed insight into the operating crystallization mechanism. The values of the Avrami exponent $n$, as calculated from the JMA plots by linear regression, reveal that there is a change in the $n$ value with the degree of thermal treatment from about 3.4 (for sample *A*) to 2.6 (for sample *D*). This observation clearly suggests that the thermal treatment in the supercooled liquid region has a strong influence on the nucleation-and-growth process. This is also substantiated by the changes in the values of the differential Avrami exponents (Fig. 6) for the different samples. In the initial stage of the transformation process the differential Avrami exponent increases. For the as-prepared sample and for the powder treated up to 708 K, this increase is essentially only up to about 10% of transformed volume, whereas it continues to about 40% and 50% for the samples treated at 733 K and 743 K, respectively. The differential Avrami exponent remains approximately constant for the as-prepared powder in the range from 10% to 95% of the transformed volume fraction. However, for the thermally treated samples the $n(X)$ values decrease significantly after about 40% of crystallization has occurred which also presents evidence that the nucleation and growth processes do not remain constant during the isothermal crystallization.

The behavior of the differential Avrami exponent $n(X)$ can be explained in the following way. Since the chemical composition of the crystallites created in the amorphous matrix differs essentially from the composition of the residual glassy material, the growth process must be diffusion controlled. The exponents obtained for the beginning of the crys-

tallization process are about 2.5 for the as-prepared powder and for the samples treated at 708 K and 733 K. This value is compatible with diffusion-controlled three-dimensional growth and a constant nucleation rate.[37] For the 743 K sample, a value of 1.6 was determined, which can be interpreted as diffusion-controlled growth of preformed nuclei.[37] This means that the isochronal treatment performed earlier at 743 K was accompanied by the formation of a large number of nuclei, which are activated at the beginning of the crystallization procedure. At lower treatment temperatures (and within the time intervals of the isochronal treatment procedure applied) the amount of preformed nuclei formed is obviously essentially lower, and for the corresponding samples continuous nucleation dominates the crystallization process already at the beginning of the isothermal treatment at 733 K. This is also substantiated by the TEM observations as seen in Fig. 9. Upon increasing the thermal treatment temperature from 708 K (sample *B*) to 743 K (sample *D*) the number density of nuclei increases.

The term $[K_T(t-t_0)]^n$ in the JMA expression (2) can also be written as $\lambda V_p$, where $\lambda$ is the number density of nuclei in the sample and $V_p$ is the mean volume of precipitated particles (e.g., Ref. 41). With three-dimensional growth the volume of a particle is proportional to $R^3$ where the particle radius $R$ grows according to $R \propto t^{1/2}$ and $R \propto t$ for diffusion- and interface-controlled growth, respectively. The number density of particles is given by the time integral over the nucleation rate. For a constant nucleation rate one obtains $\lambda \propto t$. If the nucleation rate accelerates during the process—e.g., linear increase with time—then the time integral of the nucleation rate leads to $\lambda \propto t^2$. Considering $\lambda V_p = [K_T(t-t_0)]^n$ it is clear that the increase of the differential Avrami exponents for all the samples during further annealing following the initial stage could be caused either by a qualitative change of the growth process from diffusion controlled to interface controlled or by acceleration of the nucleation process.[41] Interface-controlled growth occurs if the composition of the matrix and the precipitate are essentially the same. This does not apply to the present case because the chemical composition of the crystallites deviates essentially from the mean composition of the sample. Moreover, the difference between the compositions of crystallites and remaining amorphous matrix increases with growing volume fraction of crystallites, and diffusion keeps the process controlling the growth of particles. Therefore, acceleration of the nucleation rate must be considered to be responsible for the increase of the differential Avrami coefficient. This acceleration slows down at medium fraction of the transformed volume which is probably caused by the shift of the matrix composition towards increasing content of Ti, Ni, and Si given the fact that most of the Cu and Zr are used up in the formation of the $Cu_{51}Zr_{14}$ phase. The decrease of the differential Avrami exponent during the subsequent stage (45–90% transformed volume fraction) of crystallization is probably caused by a reduced growth rate of the crystallites. This behavior may advise the assumption that an inhibitor-controlled mechanism similar to that observed in nanocrystalline soft magnetic alloys (Finemets) becomes active above 50% of transformed volume fraction.[42] This would mean that the applicability of the JMA model and the corresponding analysis is restricted to the initial and medium stages of the crystallization processes (for details see, e.g., Refs. 43 and 44). The increase of the $n(X)$ values in the final stages of the transformation—i.e., above 95% of the transformed volume—can be attributed to a combination of various effects like errors in calorimetric measurements,[45] inhomogeneous distribution of quenched-in nuclei,[46,47] or impingement effects at the final stages of crystallization.[48]

The activation energies of the nucleation-and-growth processes controlling the crystallization of the glassy material can provide additional information on the kinetics of crystallization. The value of the activation energy calculated by the Kissinger approach for the powder in the as-prepared state (sample *A*) is comparable with the value (3.69 eV) obtained earlier for $Cu_{47}Ti_{33}Zr_{11}Ni_8Si_1$ metallic glass produced by copper mold casting.[30] The present analysis shows that the Kissinger activation energy values for all the powders are essentially the same (see Table I). The isothermal activation energy is, within the estimated error limits, equal to the Kissinger activation energy for the as-prepared powder. However, for the thermally treated samples the values obtained by the two methods differ substantially. There are two major differences. First, the isothermal activation energy is larger in magnitude than the Kissinger activation energy. Second, the isothermal activation energy increases with increased treatment temperature. It is pertinent to point out that there have been reports in which differences in the activation energy values calculated using isothermal as well as nonisothermal methods have been obtained. In Ref. 49, Köster *et al.* observed that the value of the activation energy calculated using an Arrhenius-type behavior (typically used for isothermal analysis) exceeds that determined by the Kissinger approach for a quasicrystal-forming $Zr_{69.5}Cu_{12}Ni_{11}Al_{7.5}$ glassy alloy. However, no explanation has been given for the observed difference. It has been observed in the case of a $Co_{43}Fe_{20}Ta_{5.5}B_{31.5}$ as well as the $Cu_{52.5}Ti_{30}Zr_{11.5}Ni_6$ amorphous alloy that the isothermal activation energy is substantially higher than the isochronal activation energy.[50,51] Additionally, it has been reported by the present authors that there are indeed differences in the isothermal and isochronal activation energies for the as-prepared and annealed $Cu_{47}Ti_{33}Zr_{11}Ni_8Si_1$ metallic glass powders.[36] Although all of the above reports (Refs. 36 and 49–51) mention that the observed differences can be attributed to differences in the nucleation and growth mechanisms, a convincing explanation is lacking. Conversely, it has observed that the isochronal activation energy values calculated using the Kissinger approach are larger than that calculated by isothermal analysis in the case of a $Li_2O \cdot 2SiO_2$ glass.[52] In the present study, the surprising results are that the activation energy values for the as-prepared powder are similar but are different for the thermally treated samples. In the following part of the paper an explanation of the observed differences will be given.

The activation energies are normally derived either from isothermal experiments or from Kissinger plots. In both cases it is assumed that the JMA model applies. The assumptions in the JMA model are that (i) the nucleation rate is either zero (i.e., crystallization occurs due to the growth of preexisting nuclei) or constant and (ii) growth is isotropic and is proportional to either time $t$ or $t^{1/2}$ depending on

whether the devitrification is interface or diffusion controlled.[18] (For the $t^{1/2}$ dependence, the JMA model is approximately valid.[43]) The Arrhenius plot can be done with data obtained from early transformation states whereas the Kissinger plot needs the peak temperature of the transformation event, which corresponds to a high fraction (probably about 50%) of transformed material. At such high volume fractions the applicability of the JMA model for the samples considered becomes already questionable. But even if the JMA model would apply, the Kissinger analysis will lead to incorrect results as the following calculations will show.

As displayed in Fig. 6, the formal application of Eq. (2) to the data gives an exponent $n$, which varies with the amount of transformed material. To study in detail the reason for the difference in Kissinger and Arrhenius activation energies, we simulated the Kissinger plot using the following approach. The rate constant is given by the relation (4).

For describing the experimentally observed behavior of the differential Avrami exponent $n$ (Fig. 6) the following expression was used:

$$n(X) = n_0 + a \exp[-(X - X_m)^2/2b^2], \tag{5}$$

where the parameters $n_0$, $a$, $X_m$, and $b$ were chosen in such a way that the behavior of the plots in Fig. 6 was qualitatively reproduced. For the activation energy $E$, a fixed value was inserted. Then, the first derivative of $X(t)$ was computed for a series of parameter sets, and the peak positions of the transformation process were calculated for different heating rate constants $q(T=qt)$. The estimate for the activation energy was then calculated according to the Kissinger method.

For constant exponents $n$ (not depending on $X$) the Kissinger method gave the correct result for the activation energy (4 eV assumed in the present simulation) with an error of less than 1% for the parameter range considered. For $n(X)$ varying in the range from 2 to 3 according to the above expression and Fig. 6, results for the activation energy were obtained in the range from 2.5 eV to about 5 eV (4 eV would be correct) depending on the special choice of the parameters $a$, $X_m$, and $b$—i.e., depending on the special dependence of the differential Avrami exponent on the transformed volume fraction.

From this we conclude that reliable values for the activation energy can be obtained for the present samples only from the Arrhenius plot. The fact that the Kissinger and the isothermal results agree for the as-prepared sample can, however, be easily understood, because in this case the differential Avrami exponent does not change essentially in the broad range from 10% to 95% transformed volume.

The essential change of the activation energy appears from the as-prepared sample to the one treated at 708 K. This difference is significant, whereas the slight increase of the mean values for the samples annealed at 708 K, 733 K, and 743 K remains within the error bounds and may, therefore, be questionable. Looking at the differential Avrami exponent curves in Fig. 7 the essential difference between the as-prepared powder and the thermally treated samples is observed in the middle and late stages of the crystallization process. As discussed above, this difference results from a reduced increase of the nucleation rate for the thermally treated samples compared to the as-prepared powder. Therefore, we conclude that the activation energy measured by the isothermal method reflects essentially the peculiarities of the nucleation process. It is reasonable to assume that the observed enhancement of the isothermal activation energy by prior thermal treatment is responsible for the attenuation of nucleation rates in the annealed samples. Possibly, Ti diffusion is one of the limiting factors, which is supposed by the high value of the corresponding activation energy [3.82 eV for Ti diffusion in $Fe_{40}Ni_{40}B_{20}$ compared to the value of 2.14 eV for Ni (Ref. 53)]. Additionally, it has been found that the isothermal activation energy for nucleation and growth in the $Cu_{47}Ti_{34}Zr_{11}Ni_8$ bulk metallic glass is $4.28 \pm 0.11$ eV.[54] This value is close to the value obtained for the thermally treated samples. The values are comparable to the value attributed to titanium diffusion in $Zr_{41.2}Ti_{13.8}Cu_{12.5}Ni_{10}Be_{22.5}$ metallic glass ($4.09 \pm 0.76$ eV) and suggest that the nucleation is a diffusion controlled process.[55,56]

The foregoing discussion has been based on the basis of primary crystallization. However, other factors may also have to be considered. Previous microstructural studies by the authors have found no evidence to suggest amorphous phase separation at temperatures above as well as below the observed glass transition.[33,36] However, Miller *et al.*[32] report that the $Cu_{47}Ti_{33}Zr_{11}Ni_8Si_1$ metallic glass is phase separated into two interconnected amorphous phases. These phases are copper enriched and titanium enriched. The copper-enriched regions were found to be titanium depleted and vice versa.[32] Atom probe studies are currently underway on the $Cu_{47}Ti_{33}Zr_{11}Ni_8Si_1$ metallic glass powders to look into detail if amorphous phase separation is an additional operating mechanism. Previous studies[13,16] have shown that the occurrence of such a chemical decomposition can result in an increasing nucleation rate. Another factor to be considered may be the following. The thermal treatment performed on the as-prepared powders not only result in the formation of crystalline nuclei (as visible in Fig. 9) but could also in the formation of clusters which can have a "critical" size or "undercritical" size. These clusters become "overcritical" upon subsequent reheating and grow during the crystallization process. This could also lead to the observed irregularity. In fact, it has been shown in a simulation study that the nuclei formed upon cooling an equilibrium melt and the nuclei formed upon heating an amorphous sample are exposed to different growth rates.[13]

## V. CONCLUSIONS

Thermal treatment of $Cu_{47}Ti_{33}Zr_{11}Ni_8Si_1$-gas-atomized metallic glass powders in the supercooled liquid region is shown to affect the characteristics of subsequent crystallization processes. A detailed analysis of calorimetric measurements and a discussion in terms of the differential Avrami exponent and the activation energy reveal that essentially the nucleation rates both at the beginning and in the course of the crystallization process can be affected by the prior ther-

mal treatment. The determination of the activation energies from the Kissinger and Avrami plots leads to partially controversial results. This problem is known in the literature. We found that the reason for such discrepancies is related to the type and specific features of the crystallization kinetics. Model calculations showed that reliable results for the activation energy can be obtained from both Kissinger and Arrhenius plots only if the differential Avrami $n(X)$ exponent is approximately constant during the crystallization process whereas the Kissinger method fails if $n(X)$ varies significantly with the amount of transformed volume.

**ACKNOWLEDGMENTS**

The authors thank B. Bartusch and S. Scheider for technical assistance. Funding by the German Research Foundation under Grant No. Ec 111/10-1,2 as well as by the European Union within the framework of the Research Training Network on "ductile bulk metallic glass composites" (Grant No. MRTN-CT-2003-504692) is gratefully acknowledged. Synthesis efforts by D.J.S. were supported by the U.S. Department of Energy, Basic Energy Sciences, through Iowa State University, under Contract No. W-7405-ENG-82.

*Corresponding author. FAX: +49-351-4659452. Electronic address: s.venkataraman@ifw-dresden.de

[1] R. Wagner and R. Kampmann, in *Materials Science and Technology*, edited by R. W. Cahn, P. Haasen, and E. J. Kramer (Wiley-VCH, Weinheim, 1991).
[2] M. E. McHenry, M. A. Willard, and D. E. Laughlin, Prog. Mater. Sci. **44**, 291 (1999).
[3] K. Lu, Mater. Sci. Eng., R. **16**, 161 (1996).
[4] M. T. Clavaguera-Mora, N. Clavaguera, D. Crespo, and T. Pradell, Prog. Mater. Sci. **47**, 559 (2002).
[5] J. H. Perepezko, Prog. Mater. Sci. **49**, 263 (2004).
[6] A. Inoue, A. Takeuchi, A. Makino, and T. Masumoto, IEEE Trans. Magn. **31**, 3626 (1995).
[7] L. Withanawasam, I. Panagiotopoulos, and G. C. Hadjipanayis, J. Appl. Phys. **79**, 4837 (1996).
[8] A. P. Tsai, T. Kamiyama, Y. Kawamura, A. Inoue, and T. Masumoto, Acta Mater. **45**, 1477 (1997).
[9] K. Krištiaková and P. Švec, Phys. Rev. B **64**, 184202 (2001).
[10] L. C. Chen and F. Spaepen, Nature (London) **336**, 366 (1998).
[11] H. Yinnon and D. R. Uhlmann, J. Non-Cryst. Solids **54**, 253 (1983).
[12] M. C. Weinberg, Thermochim. Acta **280/281**, 63 (1996).
[13] J. Schroers, A. Masuhr, W. L. Johnson, and R. Busch, Phys. Rev. B **60**, 11855 (1999).
[14] Y. X. Zhuang and W. H. Wang, J. Appl. Phys. **87**, 8209 (2000).
[15] J. Schroers, Y. Wu, R. Busch, and W. L. Johnson, Acta Mater. **49**, 2773 (2001).
[16] T. Waniuk, J. Schroers, and W. L. Johnson, Phys. Rev. B **67**, 184203 (2003).
[17] D. Xu and W. L. Johnson, Phys. Rev. B **74**, 024207 (2006).
[18] Q. P. Cao, J. F. Li, Y. H. Zhou, A. Horsewell, and J. Z. Jiang, Acta Mater. **54**, 4373 (2006).
[19] M. G. Scott and P. Ramachandrarao, Mater. Sci. Eng. **29**, 137 (1977).
[20] D. W. Henderson, J. Non-Cryst. Solids **30**, 301 (1979).
[21] H. E. Kissinger, Anal. Chem. **29**, 1702 (1957).
[22] A. N. Koglomorov, Izv. Akad. Nauk SSR Ser. Fiz. Mat. Nauk **3**, 355 (1937).
[23] M. W. A. Johnson and K. F. Mehl, Trans. Am. Inst. Min., Metall. Pet. Eng. **135**, 416 (1939).
[24] M. Avrami, J. Chem. Phys. **7**, 1103 (1939); **8**, 212 (1940); **9**, 177 (1941).
[25] J. W. Christian, *The Theory of Transformation in Metals and Alloys* (Pergamon Press, Oxford, 1975).
[26] A. Calka and A. P. Radlinski, in *Science and Technology of Rapidly Quenched Alloys*, edited by M. Tenhover, W. L. Johnson, and L. E. Tanner, MRS Symposium Proceedings No. 80 (Materials Research Society, Warrendale, PA, 1987), p. 203.
[27] A. Calka and A. P. Radlinski, J. Mater. Res. **3**, 59 (1988).
[28] A. Calka and A. P. Radlinski, Mater. Sci. Eng. **97**, 241 (1988).
[29] K. Lu and J. T. Wang, J. Non-Cryst. Solids **117/118**, 716 (1990).
[30] H. Choi-Yim, R. Busch, and W. L. Johnson, J. Appl. Phys. **83**, 7993 (1998).
[31] S. Venkataraman, E. Rozhkova, J. Eckert, L. Schultz, and D. J. Sordelet, Intermetallics **13**, 833 (2005).
[32] M. K. Miller, S. C. Glade, and W. L. Johnson, Surf. Interface Anal. **36**, 598 (2004).
[33] S. Venkataraman, S. Scudino, J. Eckert, T. Gemming, C. Mickel, L. Schultz, and D. J. Sordelet, J. Mater. Res. **21**, 597 (2006).
[34] M. K. Miller, Mater. Sci. Eng., A **250**, 133 (1998).
[35] S. Mechler, N. Wanderka, and M.-P. Macht, Mater. Sci. Eng., A **375-377**, 355 (2004).
[36] S. Venkataraman, W. Löser, J. Eckert, T. Gemming, C. Mickel, P. Schubert-Bischoff, N. Wanderka, L. Schultz, and D. J. Sordelet, J. Alloys Compd. **415**, 162 (2006).
[37] J. Burke, *The Kinetics of Phase Transformations in Metals* (Pergamon Press, Oxford, 1965).
[38] J. Z. Jiang, H. Kato, T. Ohsuna, J. Saida. A. Inoue, K. Saksl, H. Franz, and K. Stahl, Appl. Phys. Lett. **83**, 3299 (2003).
[39] U. Köster and U. Herold, in *Glassy Metals I, Ionic Structure, Electronic Transport and Crystallization*, edited by H. J. Guntherodt and H. Beck (Springer, Heidelberg, 1981).
[40] F. R. De Boer, R. Boom, W. C. M. Mattens, A. R. Miedema, and A. K. Niessen, *Cohesion in Metals* (North Holland, Amsterdam, 1988).
[41] H. Hermann, in *Statistical Physics and Spatial Statistics, Lecture Notes in Physics*, Vol. 554, edited by K. R. Mecke and D. Stoyans (Springer, Berlin, 2000).
[42] H. Hermann, A. Heinemann, N. Mattern, and A. Wiedenmann, Europhys. Lett. **51**, 127 (2000).
[43] P. Uebele and H. Hermann, Modell. Simul. Mater. Sci. Eng. **4**, 203 (1996).
[44] H. Hermann, N. Mattern, S. Roth, and P. Uebele, Phys. Rev. B **56**, 13888 (1997).
[45] L. Liu, Z. F. Wu, and J. Jhang, J. Alloys Compd. **229**, 90 (2002).
[46] J. C. Holzer and K. F. Kelton, Acta Metall. Mater. **39**, 1833 (1991).
[47] N. X. Sun, X. D. Liu, and K. Lu, Scr. Mater. **34**, 1201 (1996).

[48] G. Ghosh, M. Chandrasekaran, and L. Delaey, Acta Metall. Mater. **39**, 925 (1991).
[49] U. Köster, J. Meinhardt, S. Roos, and R. Busch, Mater. Sci. Eng., A **226-228**, 995 (1997).
[50] Z. Z. Yuan, X. D. Chen, B. X. Wang, and Z. J. Chen, J. Alloys Compd. **399**, 166 (2005).
[51] Y. J. Yang, D. W. Xing, J. Shen, J. F. Sun, S. D. Wei, H. J. He, and D. G. McCartney, J. Alloys Compd. **415**, 106 (2006).
[52] K. Cheng, J. Mater. Sci. **36**, 1043 (2001).
[53] F. Faupel, W. Frank, M.-P. Macht, H. Mehrer, V. Naundorf, K. Rätzke, H. Schober, S. K. Sharma, and H. Teichler, Rev. Mod. Phys. **75**, 237 (2003).
[54] S. C. Glade, J. F. Löffler, S. Bossuyt, W. L. Johnson, and M. K. Miller, J. Appl. Phys. **89**, 1573 (2001).
[55] J. F. Löffler and W. L. Johnson, Appl. Phys. Lett. **76**, 3394 (2000).
[56] E. Budke, P. Felitz, M.-P. Macht, V. Naundorf, and G. Frohberg, Defect Diffus. Forum **143**, 825 (1997).